Chaos, Solitons and Fractals 177 (2023) 114256

Contents lists available at ScienceDirect

Chaos, Solitons and Fractals

journal homepage: www.elsevier.com/locate/chaos

Epidemiological model based on networks with non-local coupling

Vitor H.A. Fávaro [a,*], Enrique C. Gabrick [b], Antonio M. Batista [b], Iberê L. Caldas [c], Ricardo L. Viana [a]

[a] Universidade Federal do Paraná, Departamento de Física, Curitiba, Paraná, Brazil
[b] Universidade Estadual de Ponta Grossa, Departamento de Matemática e Estatística, Ponta Grossa, Paraná, Brazil
[c] Universidade de São Paulo, Instituto de Física, São Paulo, São Paulo, Brazil

ARTICLE INFO

Keywords:
SIR model
Complex networks
Numerical simulations
Epidemiology

ABSTRACT

Epidemics result in loss of human lives and have a significative socioeconomic impact. In this context, epidemiological models play a crucial role in prevention and control of spread diseases. The main goal of the present work is to analyze the dispersal of an illness in a complex network of coupled sites as a function of the model parameters. Our results indicate that non-local connections lead to a quicker epidemic spread, while lower interaction between sites contributes to a slower spread. Parameters such as infection rate and initial susceptible individuals influence the epidemic dispersion, while the recovery rate and initial infected individuals at the reference site have limited impact on the disease evolution in the network.

1. Introduction

Throughout the history of humanity, various epidemics and pandemics, such as Yellow Fever, Bubonic Plague, Influenza, COVID-19, affected populations in many ways [1–4]. Some of these diseases propagate from individual to individual, whereas others are transmitted by infecting agents [5]. Disease propagation can occur by direct or indirect contact, inhalation of contaminated air, ingestion of contaminated water or food, as well as vertically transmitted diseases (from mother to child through placentae) [6].

Epidemic outbreaks are related to many determining and conditioning factors such as ecological, economic, climate, and social behavior [7–10]. Understanding such widely different factors is essential to avoid or control the propagation of diseases [11]. Mathematical models to describe epidemic propagation are valuable tools to perform these tasks, allowing the development of more efficient methods for coping with such challenges to public health and designing adequate policies [12]. Epidemic models have been considered in the study of several diseases, such as malaria, dengue, Influenza, HIV, COVID-19, among others [6,13–20].

As we know, the world is becoming increasingly interconnected, with long-distance travel allowing people to move from one place to another with notable ease. These connections, i.e. mobility, play a key role in the disease spread, as exemplified by the rapid spread of COVID-19. However, it is important to note that classical epidemiological models do not include mobility among different regions [21]. Therefore, it is essential to adapt these models by integrating a network structure, as such structures have become indispensable for the analysis of systems in social, physical, and biological contexts. Research includes the development of mathematical models to address heterogeneities within contact networks and infection dynamics, evaluating control strategies like screening and contact tracing [22].

Dynamic bipartite graphs were used to illustrate how individuals move between specific locations, shaping contact patterns [23]. Modeling network contacts helped understand the variability in Severe Acute Respiratory Syndrome (SARS) outbreaks and assess the effectiveness of public health measures [24]. A probabilistic model that combines stochastic local infection dynamics with global network transport, including civil aviation traffic, was employed to forecast the geographical spread of epidemics [25]. One study about how the diseases adapt to changing transmission routes between infected and susceptible is present in Ref. [26]. A Susceptible–Infected–Removed (SIR) model in different type of networks were studied in Ref. [27]. The authors considered variable and correlated infectivity and transmission probabilities, their results were validated through numerical simulations. Moreover, equally important research on disease spread within networks can be see in Refs. [28–44] and references therein. Moreover, given the nature of such travel, which extends beyond geographically proximate areas, models that depending solely on local couplings are insufficient for a realistic understanding of disease propagation, a remarkable way to modeling these connections is by considering complex networks [35].

* Corresponding author.
E-mail address: vitor.favaro@ufpr.br (V.H.A. Fávaro).

https://doi.org/10.1016/j.chaos.2023.114256
Received 18 September 2023; Received in revised form 2 November 2023; Accepted 8 November 2023
Available online 18 November 2023

In this work, we analyze the propagation of a disease in a network of coupled sites as a function of parameters related to the network model. In order to reach this aim, we introduce a complex network with a given number of occupied sites. The links in the network represent the interactions among individuals assigned to compartments with labels, for instance S, I or R (susceptible, infectious or recovered). The local dynamics at each site is governed by the SIR model and the coupling between sites is described by an adjacency matrix. The connection topology used is a small-world network type Newman-Watts [45–47]. This network topology is adequate to describe social dynamics, such as disease spread [48,49], because it promotes communication and interaction among diverse communities (non-local connections among the sites), offering valuable insights into comprehending intricate interactions and flows within real-world systems. It essentially aids in grasping the global-scale impact of local decisions and behaviors and how non-local events influence local communities.

We characterize quantitatively the propagation of the disease along the network by an average advance time computed from the times at which each site reaches a maximum number of infected individuals. Another quantity numerically computed is the extinction time, which measures how long it takes for a large fraction of the population to be recovered from the disease. The network parameters to be considered are the probability of non-local shortcuts, the coupling strength, and the basic reproduction number.

In this paper, we show that Newman-Watts networks exhibit lower extinction times for epidemics compared to regular networks. Furthermore, the strength of coupling plays a fundamental role in the epidemic's spread, where higher levels of interaction lead to shorter extinction times. When examining the infection rate and the initial susceptible individuals, it becomes evident that these factors affect the epidemic dispersion. In contrast, the recovery rate and the initial infected individuals at the reference site have a relatively minor impact on the progression of the disease.

The paper is organized as follows. In Section 2, we outline the mathematical model for the complex network of sites, each of them governed by the SIR equations. Section 3 contains the results of numerical simulations, where we consider the effects of the coupling and network parameters on the quantities mentioned, which are relevant from the epidemiological point of view. The last Section is devoted to our Conclusions.

2. Network model

The Susceptible–Infected–Recovered (SIR) model is a compartmental model widely used in mathematical modeling of infectious diseases [6,14,15,18,50]. In this model, the host population (N_H) is divided into compartments namely $S(t)$, $I(t)$, and $R(t)$ which represents the number of susceptible, infected, and removed individuals, respectively. The number of individuals belonging to each class varies with time, reflecting the dynamics of disease propagation.

When a susceptible individual meets an infectious individual, the former may contract the disease and becomes infected. The contamination rate β describes the transition of individuals from susceptible to infected. The removed individuals are either recovered from the disease or deceased. The corresponding recovering rate is denoted by α, corresponding to those infectious individuals that recover from the disease.

The differential equations governing the evolution of these variables in the SIR model are

$$\frac{dS}{dt} = -\beta SI, \tag{1}$$

$$\frac{dI}{dt} = \beta SI - \alpha I, \tag{2}$$

$$\frac{dR}{dt} = \alpha I. \tag{3}$$

The evolution of the system starts with an initially small number of infected individuals that contaminate susceptible individuals with whom they establish contact, such that the number of infected individuals increases to a maximum. After that, it decreases as individuals recover and enter into the removed category. Since the total population $S + I + R$ is constant, its rates satisfy

$$S'(t) + I'(t) + R'(t) = 0, \tag{4}$$

for any time, where the notation $F'(t)$ indicates dF/dt.

The temporal evolution of the disease can be quantitatively described by the so-called basic reproduction number, defined by

$$R_0 = \frac{\beta S(0)}{\alpha}, \tag{5}$$

where $S(0)$ is the initial number of susceptible individuals. The parameter R_0 indicates the average number of secondary infectious individuals from a single individual introduced in a susceptible population [6,51]. If $R_0 > 1$, there is a possibility of an epidemic outbreaks, since a single infectious individual is enough to produce this effect. On the other hand, if $R_0 < 1$, the conditions are unfavorable to the propagation of the disease.

The Eqs. (1)–(3) are strictly applicable only within an isolated environment, where the total population remains constant [50]. However, when considering a system composed of multiple communities connected through transportation, the movement of individuals through these transport channels becomes an important factor. Infected individuals can depart their community and travel to others, where they may infect susceptible individuals. Likewise, susceptible individuals can become infected by traveling to communities where the disease has already spread. These matters have received significant attention recently, particularly due to the rapid transmission of COVID-19 facilitated by extensive transportation between countries and continents.

The theoretical study of spatial propagation of epidemics can be done in various ways, reflecting specific realities and scenarios of disease propagation. In a recent paper Mugnaine et al. have investigated the spatial evolution of a disease using a SEIR model based on stochastic cellular automata where the interaction of adjacent cells is represented by a set of evolution rules [52].

Another approach is to use complex networks to describe the spatial propagation of epidemics. In this theoretical framework, we consider that individuals are mainly attached to spatially localized communities that are linked by roads or other forms of transport, used by individuals to go from one community to another. In principle, this model would require a relatively simple network, where each site is connected only to its closest neighbors. While this assumption holds true for purely terrestrial transport, it is also possible to incorporate aerial or maritime transportation, which can connect geographically distant sites. The latter aspect demands a non-local network structure, involving shortcuts that connect nearest neighbors [32,41,43,53–64].

Non-local connections can be implemented in a complex network using a connectivity matrix $\mathbf{A}$ with elements $A_{ij} = 1$ if the sites i and j are connected by a link, and 0 otherwise. A further improvement would be to include weights in the links that are proportional to the connection strength, however this possibility will not be explored in this work. There is an extensive number of quantifiers to characterize the structure of complex networks, but we are particularly interested in two of them: the average path length ℓ and the clustering coefficient C. The former is the average number of connections required to go from one site to another. The clustering coefficient is defined as the probability that two sites are connected given that they share a connection with a third one.

Regular networks, which present nearest neighbor connections only, have relatively large values for both ℓ and C, since it takes many links on average to go from one site to another. Moreover, the clustering is large since we can draw an extensive number of triangles of neighbors. On the other hand, random networks (type Erdös-Renyi) have links randomly assigned to sites according to a given probability. For them, both ℓ and C are small.

In the present work, we use a complex network of the Newman-Watts type, exhibiting the small-world property, i.e., the average path

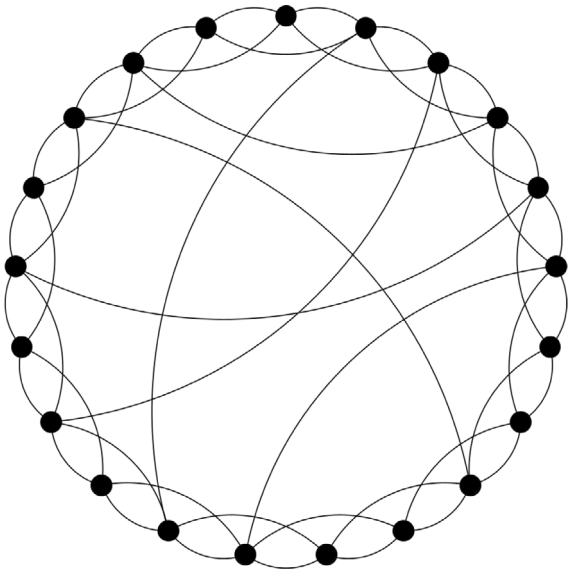

Fig. 1. Schematic representation of a Newman-Watts network with $N = 21$ and $p = 0.3$.

length between sites is relatively small, while retaining a considerable amount of clustering [46,47,65–67]. In this type of small-world network, we start from a regular lattice of N sites with connections to their nearest and next-to-the-nearest neighbors, and we attach a small number of shortcuts chosen with probability p [46,47]. The regular part of the lattice is responsible for the relatively large clustering $C \gg C_{random}$, whereas the shortcuts stand for the relatively small average path length $\ell \sim \ell_{random}$. The corresponding connectivity matrix has several diagonals filled with ones, parallel to the main diagonal filled with zeros (since a site cannot connect with itself), and the shortcuts are ones randomly scattered among the rest of the matrix.

We denote $S_j(t)$, $I_j(t)$, and $R_j(t)$ the numbers of susceptible, infectious, and removed individuals in a site j, where $j = 1, 2, 3, \ldots, N$, at a given time t. Since there is a continuous exchange of individuals among sites, these values are expected to vary with time. We have chosen a small-world network to couple the communities since it is reasonable that most people commute by terrestrial means, whereas only a small fraction of them use aerial transport. Fig. 1 shows a schematic of the small-world network used in this work. We adopt periodic boundary conditions in the regular part of the lattice.

In the network model, each site is considered as a population governed by the SIR model and the coupling is given by the connectivity matrix, which describes the small-world architecture. To incorporate interaction between these sites, we assume that a fraction of individuals from each class has the ability to migrate to other locations in the network. Based on these assumptions, our model is given by:

$$\frac{dS_j}{dt} = -\beta S_j\, I_j - D\left[S_j - B_j \sum_{i=1}^{N} A_{ji}\, S_i\right], \tag{6}$$

$$\frac{dI_j}{dt} = \beta S_j\, I_j - \alpha I_j - D\left[I_j - B_j \sum_{i=1}^{N} A_{ji}\, I_i\right], \tag{7}$$

$$\frac{dR_j}{dt} = \alpha I_j - D\left[R_j - B_j \sum_{i=1}^{N} A_{ji}\, R_i\right], \tag{8}$$

where D characterize the coupling strength in day^{-1}, B_j is a normalization parameter associated with each site, and A_{ij} is the connectivity matrix. If $A_{ji} = 1$, then i is connected with j, and $A_{ji} = 0$ otherwise. In addition, $A_{ij} = 0$ if $i = j$, i.e. self-connections are excluded. The normalization parameter is given by

$$B_j = \left(\sum_{i}^{N} A_{ji}\right)^{-1}. \tag{9}$$

To understand the network model dynamics, consider Eq. (6) and the susceptible individuals at site 501. From Eq. (6), it is valid to state that some of the susceptibles at site 501 migrate to other sites, based on a connectivity matrix that facilitates the interaction of individuals from different communities. Simultaneously, susceptibles from other sites migrate to site 501, influenced by the coupling intensity D. This approach gives a network of interactions among different communities. The same argument can be extended to Eqs. (7) and (8).

As a mentioned, the sum of the classes represents the host population N_H, for each site in the network. Thus, we can verify that the total population of the network is given by

$$\sum_{j=1}^{N}(S_j + I_j + R_j) = M, \tag{10}$$

where M stands for the total population of the network. Additionally, we observe that their rates comply

$$\sum_{j=1}^{N}(S_j' + I_j' + R_j') = \Gamma. \tag{11}$$

Consequently, we can ascertain that

$$\Gamma = -D\sum_{j=1}^{N}\left[S_j + I_j + R_j - B_j \sum_{i=1}^{N} A_{ji}(S_i + I_i + R_i)\right] = 0, \tag{12}$$

indicating that the total population of the network remains constant at all times. However, it is worth noting that this constraint limits the equations model used, since the coupling intensity D, infection rate β, and recovery rate α would ideally vary among different network sites to provide a more realistic scenario. Nevertheless, analyzing this model with many variable parameters initially could make the assessment of results challenging or even unfeasible. Consequently, we chose to simplify the model to allow for the analysis of a larger number of parameters in the initial stages.

The coupled system of Eqs. (6)–(8) is numerically solved by using a fourth-order Runge–Kutta method. The code is implemented in Python using the library *solve-ivp* [68]. The timestep is fixed in 0.01. The numerical values of the parameters have been used as $\beta = 0.002342$ day^{-1} and $\alpha = 0.476$ day^{-1}, which were taken from a study related to Influenza A [6]. We consider $N = 1001$ sites, each of them initially with 1000 susceptible individuals, except the site $j = 501$, for which we put a single infectious individual, with the remaining 999 susceptible individuals.

3. Results

In order to analyze the dispersion of the disease along the complex networks, we introduce two quantifiers. The first, denoted as advancement rate, measures the velocity at which the illness spreads in the network. Fig. 2 is an illustration of three different infected curves in three different sites, namely, $j-1$, j, and $j+1$. The distance between two sites is given by Δx and the time interval in which each peak ($I_{\max}$) occurs is Δt. Note that, peak time is the time at which the infected individuals curve reaches its maximum value, while the peak time interval refers to the time between two maxima in different sites. In this way, the advancement rate is $T = |\Delta x|/|\Delta t|$. We consider $|\cdot|$ to ensure the positivity of T. Consider, for example, the site $j-1$ and the central site j. In this case the distance is $\Delta x = (j-1) - j$, the time interval is $\Delta t = (t_{j-1}) - t_j$, and the advancement rate is $T = 1/|(t_{j-1}) - t_j|$. Similarly, to the $j+1$ site we obtain $T = 1/|(t_{j+1}) - t_j|$.

Similarly to the previous procedure, we generalize T for the whole network. For this, we consider the reference site j and its neighbors represented as $j+n$ and $j-n$, where $n = 1, 2, 3, \ldots, (N-1)/2$ for a network consisting of an odd number of N sites. The reference site is the initial node containing infected individuals. The distance Δx is defined by $\Delta x = |(j \pm n) - j|$. The time interval ($\Delta t$) represents the difference in peak times between the sites $j \pm n$ and j. Consequently, we define the

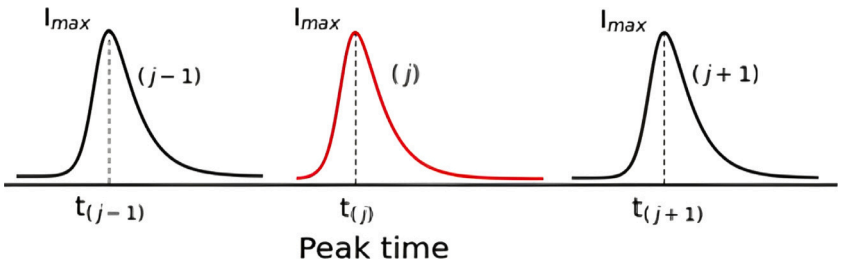

Fig. 2. Illustration of the time at which each site on the network reaches the infected curve peak.

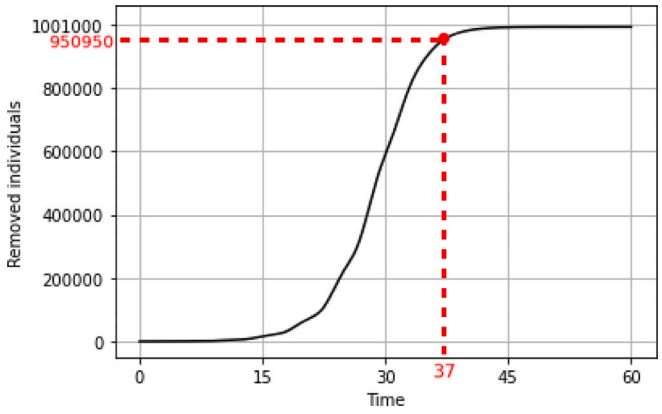

Fig. 3. Illustration of the epidemic's extinction time, where the dashed red lines indicate how long it took for 95% of the population transition to the removed class.

peak times as follows: t_j for site j; $t_{(j+n)}$ for site $j+n$; and $t_{(j-n)}$ for site $j-n$. Therefore, we express the advancement rate magnitude at which the disease reaches site $j \pm n$ as:

$$T_{(j\pm n)} = \frac{|(j \pm n) - j|}{|t_{(j\pm n)} - t_j|} = \frac{|\pm n|}{|t_{(j\pm n)} - t_j|}. \tag{13}$$

Intending to analyze the advancement across the complex network, we choose to calculate its average by

$$T_m = \frac{1}{n_t} \sum_{i=1}^{n_t} T_i, \tag{14}$$

where T_i corresponds to the advancement rate of each site, while n_t represents the number of sites affected by the epidemic, excluding the reference site. The average is calculated after the disease has reached all sites in the network, that is, obtain all the values of T_i, and then we calculate the average of the rates. Throughout the article, we refer to the rate defined by Eq. (14) as the average epidemic's advancement rate.

As is commonly understood, when an infectious disease spreads within a population, it affects individuals who are susceptible to infection, and those who become infected and later recover are categorized as removed individuals. Based on the number of recovered individuals, in this study, we introduce a second quantifier to analyze, called the epidemic's extinction time.

In this research, we characterize the epidemic's extinction time as the moment at which the disease is considered extinct, signifying that the majority of the population has already been recovered. To do this, we define the moment when the disease is considered extinct as the point at which 95% of the total population within the network has transitioned into the removed category.

In Fig. 3, we illustrate how the number of removed individuals in the network increases as infected individuals recover, allowing us to estimate the epidemic's extinction time for a population of 1001 sites, each with $N_H = 1000$ individuals.

It is important to clarify that, from a mathematical perspective, this does not necessarily mean that the disease has entirely vanished. Instead, it signifies the absence of an active outbreak, with only minimal new infections occurring. In summary, the epidemic's extinction time is when the majority of infected individuals have successfully recovered, leading to a significant reduction in the disease's spread.

Moreover, for each set of parameters, we run the program 100 times for $0 < p \leq 1$, calculating the results as the average of these runs. This approach was adopted due to the variation in the adjacency matrix with each execution, resulting in more accurate and representative results. In this way, to assess the variability of the outcomes, we establish error bars based on the standard deviation calculated from an average of 100 samples. Additionally, we must emphasize that the curves' captions containing the coupling strength value D have their units omitted, which are day^{-1}.

In Fig. 4, we observe a significant change in the epidemic's extinction time when adding non-local connections, transitioning from a regular network ($p = 0.0$) to a Newman-Watts type network ($0 < p \leq 1$). The panel (a) exhibit the epidemic's extinction time as function of p, including $p = 0.0$, while the panel (b) display an amplification of panel (a) considering $p > 0.0$. Our results indicate that for high values of p, the disease extinguished more rapidly, revealing a significant impact of introducing non-local connections on the dynamics of disease propagation.

Observing Fig. 5, which illustrates the average epidemic's advancement rate as a function of the probability p, we notice that the rate increases as the values of p become higher. What indicates that the higher the probability of adding non-local connections, the greater the average epidemic's advancement rate. Furthermore, it is interesting to note that the error associated with the numerical results remains similar for most values of p, except when $p = 0.0$. This difference in the error for $p = 0.0$ attributed to the absence of non-local connections, resulting in homogeneity in the results.

In Fig. 6, we maintain the parameter p fixed and varied the coupling intensity D. This allow us to observe that the epidemic's extinction time reduced as the coupling intensity D between network sites increased. In other words, the more intense the coupling is, faster the epidemic spreads throughout the network.

Fig. 7 shows that the average epidemic's advancement rates are lower when the interaction intensities D between sites are lower. This result complements the pattern observed in Fig. 6 and suggests that reduced interaction intensities among sites not only lead to longer extinction times but also contribute to slower disease spread within the population.

The numerical results presented in Figs. 4–7 emphasize the importance of the quantity of non-local connections and the intensity of coupling in the context of the epidemic. The probability of introducing non-local connections p, plays a significant role in the mobility between different geographical regions. A high value of p implies a considerable increase in population mobility, driven by factors such as migration, and temporary or permanent relocations of individuals, among others. This heightened mobility naturally intensifies the spread of the disease, as the illness finds more opportunities to disseminate through interactions among individuals. In such cases, people are more likely to

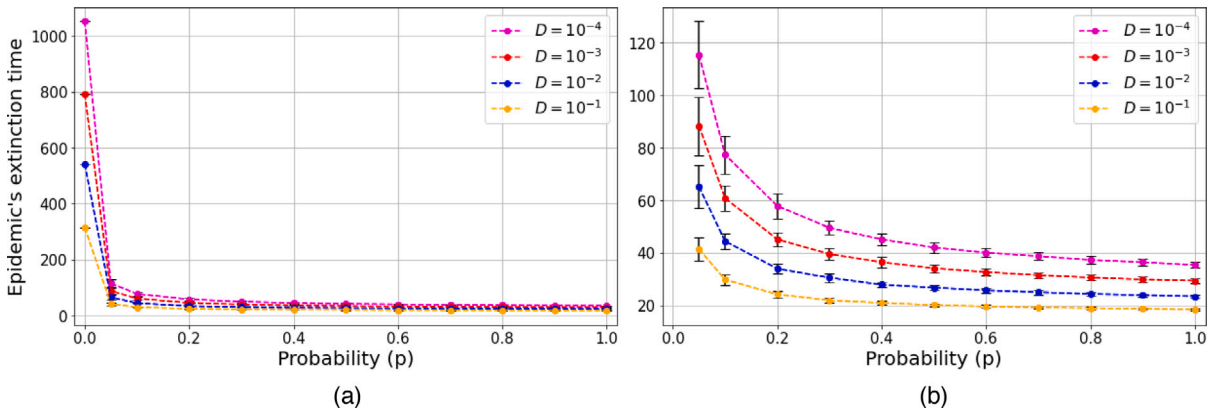

Fig. 4. Time at which the epidemic extinguished from the network as a function of p for (a) $p = 0.0$ and (b) $p > 0.0$. We consider $N_H = 1000$, $\beta = 0.002342$ day^{-1} and $\alpha = 0.476$ day^{-1}.

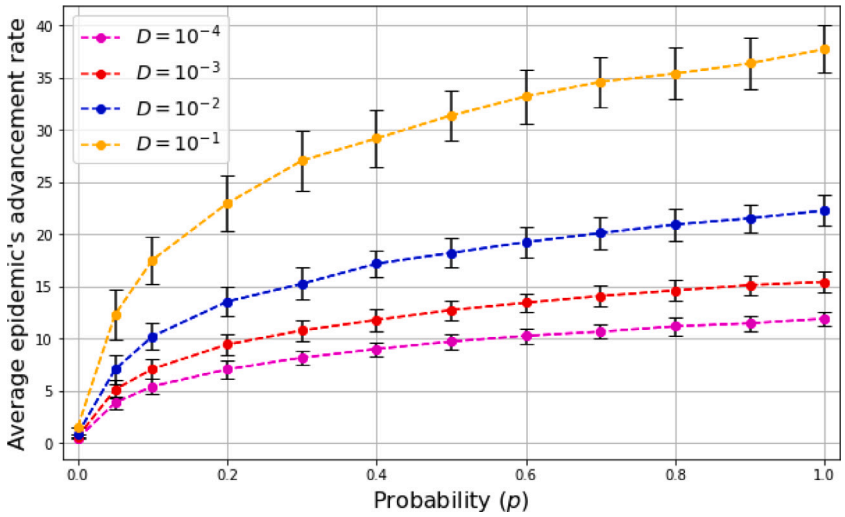

Fig. 5. Average epidemic's advancement rate as a function of p. We consider $N_H = 1000$, $\beta = 0.002342$ day^{-1} and $\alpha = 0.476$ day^{-1}.

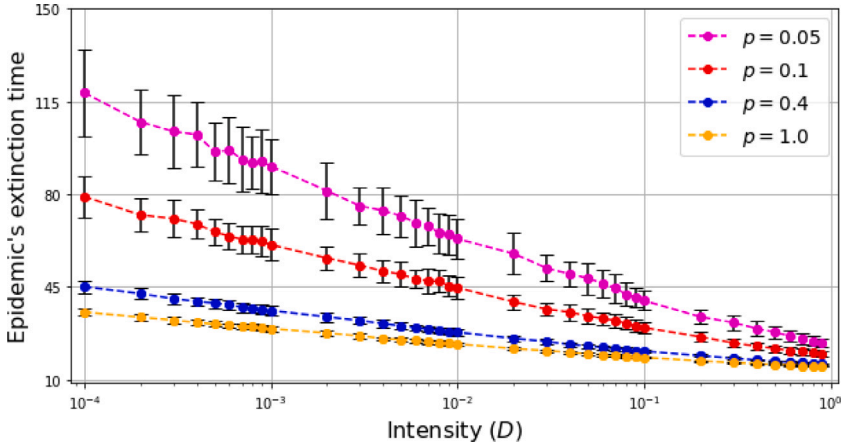

Fig. 6. Time at which the epidemic extinguished from the network as a function of coupling intensity D. We consider $N_H = 1000$, $\beta = 0.002342$ day^{-1} and $\alpha = 0.476$ day^{-1}.

come into contact with disease carriers or locations where the disease is already present.

On the other hand, a low value of p indicates that regions are weakly connected or that control measures have been implemented, such as the closure of borders between cities or countries. Resulting in reduced population mobility between different communities, which leads to a slower spread of the epidemic. The reduction in mobility can contribute to the control or even the extinction of the disease, as opportunities for contact between infected and susceptible individuals are substantially reduced. This is similar to scenarios in which containment measures are highly effective, leading to a significantly lower transmission rate and enabling more effective epidemic control.

Meanwhile, when the coupling intensity D is high, the disease tends to spread rapidly and extensively within the population. Aligning with

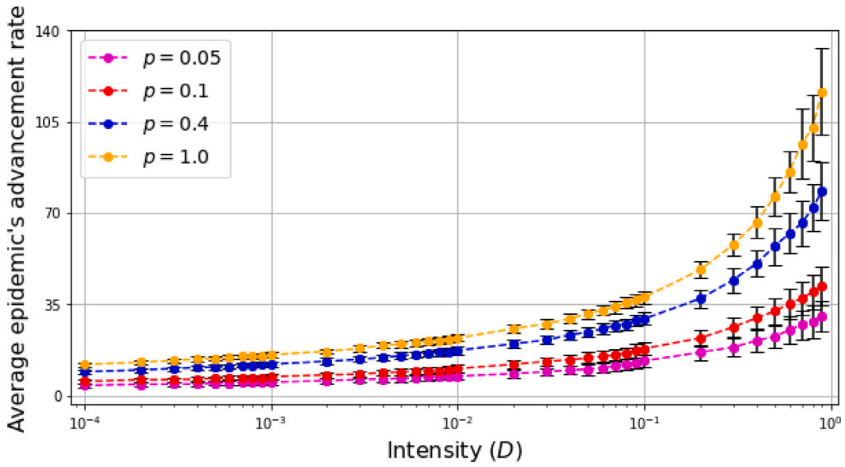

Fig. 7. Average epidemic's advancement rate as a function of coupling intensity D. We consider $N_H = 1000$, $\beta = 0.002342$ day^{-1} and $\alpha = 0.476$ day^{-1}.

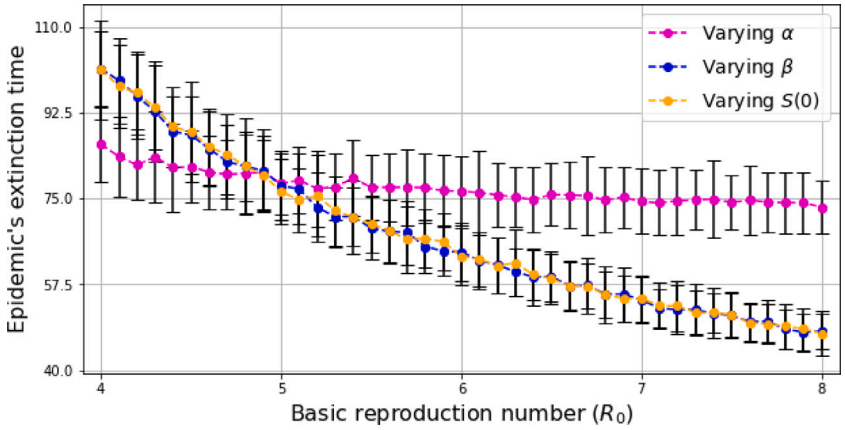

Fig. 8. Time at which the epidemic extinguished from the network as a function of basic reproduction number R_0. We consider $p = 0.1$ and $D = 10^{-4}$ day^{-1}.

what we often observe in real-world, where the absence of control measures such as social isolation and quarantine allows the disease to propagate quickly. In these situations, the interaction among individuals are not adequately controlled to contain transmission, resulting in the disease spreading through close contacts, gatherings in crowded places, or social events, which can overwhelm healthcare systems.

In contrast, for low values of D, the spread of the epidemic occurs at a slower pace, increasing the probability of controlling or extinguishing the disease. These measures occur in scenarios where highly effective containment measures are implemented, leading to a significant reduction in the transmission rate. We must emphasize that not only does it decrease the number of infected cases but also alleviates the strain on healthcare resources, enabling a more efficient control of the epidemic.

Through these results, we observe that higher values of p and greater coupling intensities D are associated with a higher spread of the disease. This finding has significant implications for understanding the impact of social connectivity and mobility on epidemic dynamics. Moreover, it accentuates the importance of considering local and global interactions in designing effective strategies for epidemic control and prevention.

Now, to understand the impact of the infection rate β, recovery rate α, and the initial number of susceptible individuals in the network on the spread of the disease, we employ the basic reproduction number, denoted as R_0 and defined in Eq. (5). To achieve this, we maintain p and D at constant values and vary each parameter contributing to R_0. This methodology furnish us with a means to gain insights into the epidemic's dynamics and pinpoint the pivotal factors that significantly shape its epidemiological outcomes.

Additionally, we investigate the influence of the initial quantity of infected individuals at the reference site $j = 501$, at $t = 0$, denoted as $I_{501}(0)$. Understanding how changes in this initial condition affect disease spread further enrich our analysis and contribute to a comprehensive understanding of the epidemic dynamics.

Fig. 8 illustrates the epidemic's extinction time as a function of the basic reproduction number R_0, considering variations in the infection rate β, the recovery rate α, and the initial number of susceptible individuals in the network $S(0)$. Thus, we find that increasing the infection rate β leads to a decrease in the extinction time of the epidemic, indicating an influence of β on the necessary period for the epidemic to be extinguished from the network. Similar results were obtained when varying the number of susceptible individuals $S(0)$. Furthermore, when fixing β and $S(0)$ and varying only the recovery rate α, there is no significant difference in the epidemic's extinction time within the analyzed range. This suggests that the recovery rate may not be a critical factor in determining the epidemic's duration under these conditions.

In essence, the variation in α does not significantly impact the time that epidemic dissipates. This insight prompts us to consider that, in certain instances, the rate at which individuals recover from the infection may not be a pivotal determinant in shaping the temporal dynamics of the epidemic. Instead, factors like transmission rate β, the number of susceptible individuals $S(0)$, and the broader network structure might play more prominent roles in the disease's dispersion.

The results presented in Fig. 9 support the previous discussions, showing that the parameters β and $S(0)$ have a significant impact on both the epidemic's extinction time and the average epidemic's

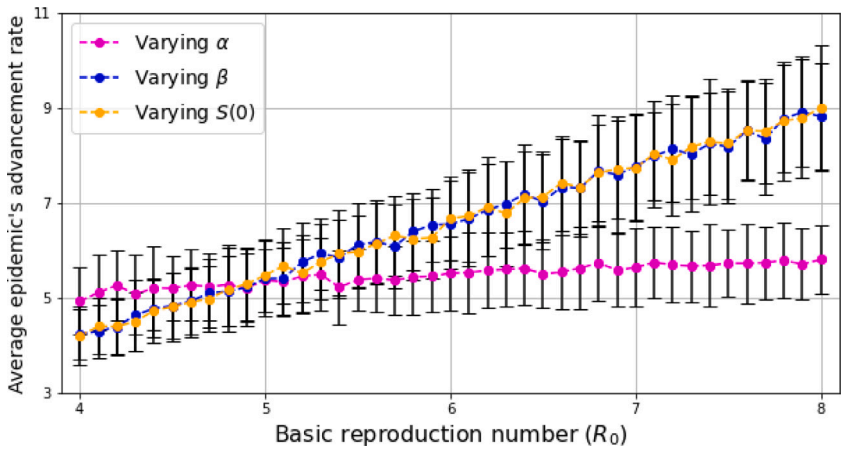

Fig. 9. Average epidemic's advancement rate as a function of basic reproduction number R_0. We consider $p = 0.1$ and $D = 10^{-4}$ day^{-1}.

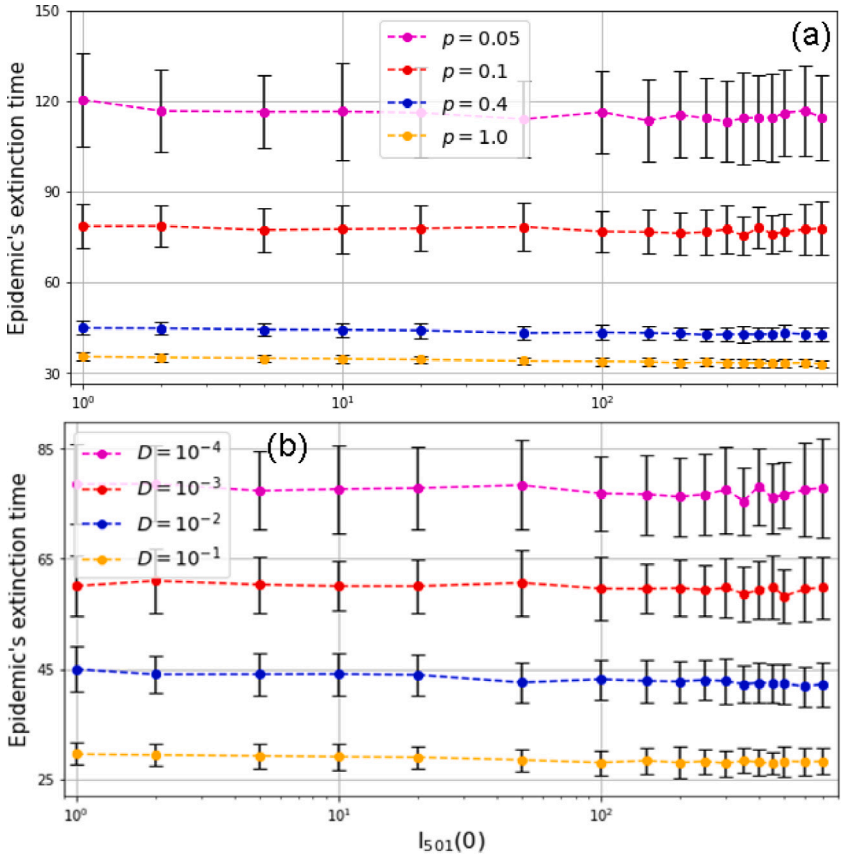

Fig. 10. Time at which the epidemic extinguished from the network as a function of $I_{501}(0)$ for (a) $D = 10^{-4}$ day^{-1} and (b) $p = 0.1$. We consider $N_H = 1000$, $\beta = 0.002342$ day^{-1} and $\alpha = 0.476$ day^{-1}.

advancement rate. We also observe that the parameter α has a less influence compared with the other ones, as its variation is within the range of fluctuations of the results.

In Fig. 10, we observe that the initial quantity of infected individuals at the reference site $j = 501$ does not have a relevant influence on the epidemic's extinction time. The initially presented result is surprising and counter-intuitive, as we might expect that a higher initial number of individuals infected at site $j = 501$ at $t = 0$ would lead to more individuals being transmitted to the interconnected network sites, resulting in a potentially shorter epidemic extinction time. However, an alternative interpretation of this result reveals that the augmentation in the number of infected individuals at the reference site has no impact on the transmission dynamics, which is due to the overriding influence of the parameters β and $S(0)$ in this process, as previously observed.

The findings presented in Fig. 11 serve as a complementary perspective to those illustrated in Fig. 10. Given that the epidemic's extinction time remained consistent, it follows that variations in the initial number of infected individuals at the reference site $j = 501$ should not alter the average rate of epidemic progression, as evidenced.

The absence of an impact from the initial number of infected individuals at the reference site on extinction time and the average rate of epidemic progression suggests that other network characteristics, holds a more significant influence on disease spread. Nevertheless, it is essential to factor in the specific context and unique attributes of the studied disease for a more precise interpretation.

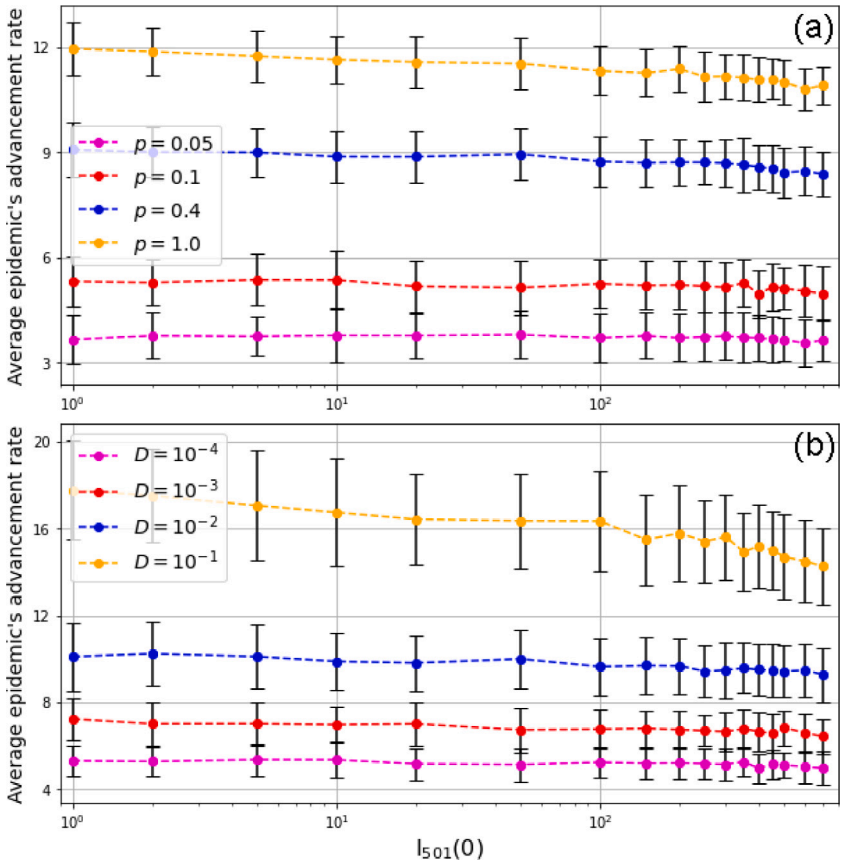

Fig. 11. Average epidemic's advancement rate as a function of $I_{501}(0)$ for (a) $D = 10^{-4}$ day^{-1} and (b) $p = 0.1$. We consider $N_H = 1000$, $\beta = 0.002342$ day^{-1} and $\alpha = 0.476$ day^{-1}.

4. Conclusions

In this article, we study the disease spread in Newman-Watts network where the shortcuts simulate the mobility. Our results show that Newman-Watts network exhibit lower extinction times for epidemics compared to regular networks. Furthermore, we verified that the average epidemic's advancement rate increases with higher values of shortcuts probability p. This occurs because as measured more infected individuals transit in the network more individuals get the infection [48,49,52]. Similarly, the epidemic's extinction time decreases as we introduce non-local connections. This results emphasizes the intricate interplay of network topology and connectivity in influencing the course of epidemics [34,35].

In relation to the influence of interaction intensity within the network, we have found that an increase in the coupling intensity D directly correlates with a decrease in the time to epidemic extinction. Furthermore, as interaction intensities between sites decrease, the average epidemic's advancement rate also reduces. These observations collectively highlights the critical role of interaction intensity in the epidemic dynamics within the network.

When considering the impact of parameters related to the equation, we verified that increasing the infection rate β, led to a shorter extinction times. Similarly, when we increased the number of susceptible individuals $S(0)$ in the network, we observed higher values for the average epidemic advancement rate. However, our findings related to the recovery rate α are counter-intuitive. We might expect that as α increases, the extinction time decreases because the individuals are sending to removed compartment faster. Nevertheless, this is not true on the analyzed interval. The examined α values suggest that lower values have a lesser impact on the spread of the disease. We must emphasize that the number of susceptible individuals in the network changes as the value of α varies after the epidemic. Specifically, a higher value of α, indicating that individuals recover more rapidly from the disease, results in fewer infections within the network. Consequently, this leads to a higher number of susceptible individuals at the end of the epidemic. Thus, it is important to highlight that these findings about the impact of α on the disease dispersion are applicable within the examined range of values.

The second counter-intuitive result is that the initial infected number in the central site does not play a crucial mechanism in the disease spread. This occurs because the extinction time depends on the transitions between sites. If we have a large amount of initial infected in a certain site, only a given fraction will transit in the network, and it is these transitions that determine the time to extinction. These findings contribute to the advance of understanding the spread of diseases in networks.

In summary, our results underscore the interplay of network structure, interaction intensity, and equation-related parameters in shaping the dynamics of epidemic propagation. The complex interactions and dependencies on epidemic dispersion observed in this study provide essential insights for devising more informed strategies to contain and mitigate epidemics within real-world networks.

Given we cannot observe the spatial movement of these individuals, who are currently evenly distributed across the area, this uniform distribution fails to capture the dynamics of real-world scenarios. As people routinely migrate between geographic regions and engage in varying levels of interaction, this mobility significantly influences the spread of diseases [39–42,44]. To ensure the continuity of our research, we propose introducing spatial heterogeneity in the network, considering distinct values for the intensity of interactions D among individuals in specific network sites. This approach will allow for a more realistic investigation of disease spread in different regions or locations within the network, potentially revealing patterns that would not be evident in a homogeneous approach.

Since the role of individuals in disease progression remains unknown, traditional compartmental models treat the population as a monolithic entity, neglecting individual variations among classes. We suggest considering the diverse characteristics of individuals at each site, establishing different values for infection rates β and recovery rates α at selected sites. With this approach, it will be possible to assess how disease spread would occur, taking into account the potential individual responses to disease progression at each site, due to the unique characteristics of each population.

Finally, it is essential to explore other epidemiological models to better understand disease dissemination in a complex network. This can be done by including a mortality rate for individuals or by defining a period during which reinfection of a recovered individual is possible. We believe that the continuation of this research will provide a new perspective on the temporal evolution of diseases, enabling a more accurate understanding of this dynamic in complex networks.

CRediT authorship contribution statement

Vitor H.A. Fávaro: Data curation, Formal analysis, Investigation, Methodology, Validation, Visualization, Writing – original draft, Writing – review & editing. **Enrique C. Gabrick:** Formal analysis, Methodology, Validation, Writing – review & editing. **Antonio M. Batista:** Formal analysis, Methodology, Validation, Writing – review & editing. **Iberê L. Caldas:** Formal analysis, Methodology, Validation, Writing – review & editing. **Ricardo L. Viana:** Conceptualization, Formal analysis, Funding acquisition, Investigation, Methodology, Project administration, Resources, Software, Supervision, Validation, Writing – review & editing.

Declaration of competing interest

The authors declare that they have no known competing financial interests or personal relationships that could have appeared to influence the work reported in this paper.

Data availability

Data will be made available on request.

Acknowledgments

The authors thank the financial support from the Brazilian Federal Agencies (CNPq) under Grant Nos. 404120/2022-9, 403120/2021-7, 301019/2019-3; the São Paulo Research Foundation (FAPESP, Brazil) under Grant Nos. 2022/04251-7, 2018/03211-6 and support from Coordenação de Aperfeiçoamento de Pessoal de Nível Superior (CAPES), Brazil under Grants No. 88887.143103/2017-01. E.C.G. received partial financial support from Coordenação de Aperfeiçoamento de Pessoal de Nível Superior (CAPES), Brazil - Finance Code 88881.846051/2023-01. We acknowledge useful discussions with Sabrina Borges Lino Araujo (UFPR), and Jane Rosa (IFPR), as well as the computational support from Carlos de Carvalho (UFPR).

References

[1] Chippaux JP, Chippaux A. J Venom Anim Toxins Including Trop Dis 2018;24.
[2] Glatter KA, Finkelman P. Amer J Med 2021;134:176–81.
[3] Dushoff J, et al. Proc Natl Acad Sci 2004;101(48):16915–6.
[4] Brugnago EL, et al. Chaos Solitons Fractals 2020;140:110164.
[5] Bhatt S, et al. Nature 2013;495(7446):504–7.
[6] Martcheva M. An introduction to mathematical epidemiology. 1st ed.. Gainesville: Springer; 2015.
[7] Abreu FVSd, et al. Parasites Vectors 2022;15(1):1–18.
[8] Qiu Y, Chen X, Shi W. J Popul Econom 2020;33:1127–72.
[9] Morin CW, Comrie AC, Ernst K. Environ Health Perspect 2013;121(11–12):1264–72.
[10] Weiss RA, McMichael AJ. Nat Med 2004;10(Suppl 12):570–6.
[11] Dai J, et al. Processes 2020;9(1):55.
[12] Anderson RM, May RM. Infectious diseases of humans: dynamics and control. Oxford University Press; 1991.
[13] Hoshen MB, Morse AP. Malaria J 2004;3:1–14.
[14] Esteva L, Vargas C. Math Biosci 1998;21, Elsevier.
[15] Kermack WO, McKendrick AG. Proc R Soc Lond Ser A 1927;155:700–21.
[16] Aguiar M, et al. J Theoret Biol 2011;289:181–96.
[17] Dalal N, Greenhalgh D, Mao X. J Math Anal Appl 2008;341(2):1084–101.
[18] Murray JD. Mathematical Biology: I. An Introduction. 3rd ed.. New York: Springer; 2002.
[19] Cooper I, Mondal A, Antonopoulos CG. Chaos Solitons Fractals 2020;139:110057.
[20] Keeling MJ, Grenfell BT. Proc R Soc Lond 2002;269(1489):335–43.
[21] Batista AM, et al. Rev Bras Ensino de Física 2021;43:e20210171.
[22] Eames KTD, Keeling MJ. Proc Natl Acad Sci 2002;99(20):13330–5.
[23] Eubank S, et al. Nature 2004;429(6988):180–4.
[24] Meyers LA, et al. J Theoret Biol 2005;232(1):71–81.
[25] Hufnagel L, Brockmann D, Geisel T. Proc Natl Acad Sci 2004;101(42):15124–9.
[26] Read JM, Keeling MJ. Proc R Soc B 2003;270(1516):699–708.
[27] Newman MEJ. Phys Rev E 2002;66(1):016128.
[28] Ferguson NM, et al. Nature 2006;442(7101):448–52.
[29] Wallinga J, Edmunds WJ, Kretzschmar M. Trends Microbiol 1999;7(9):372–7.
[30] Liu J, Tang Y, Yang ZR. Trends Microbiol 2004;2004(08):P08008.
[31] Boccaletti S, et al. Phys Rep 2006;424(4–5):175–308.
[32] Keeling MJ, Eames KTD. J R Soc Interface 2005;2(4):295–307.
[33] Pastor-Satorras R, Vespignani A. Phys Rev Lett 2001;86(14):3200.
[34] Pastor-Satorras R, Vespignani A. Phys Rev E 2001;63(6):066117.
[35] Pastor-Satorras R, et al. Phys Rev E 2015;87(3):925–79.
[36] Colizza V, et al. PLoS Med 2007;4(1):e13.
[37] Tatem AJ, Rogers DJ, Hay SI. Adv Parasitol 2006;62:293–343.
[38] Belik V, Geisel T, Brockmann D. Phys Rev X 2011;1:5.
[39] Barmak DH, Dorso CO, Otero M. Physica A 2015;447:129–40.
[40] Findlater A, Bogoch II. Trends Parasitol 2018;34(9):772–83.
[41] Rüdiger S, et al. Sci Rep 2020;10(1):5919.
[42] Du B, et al. Int J Data Sci Anal 2021;12:369–82.
[43] Du M. Sci Rep 2021;11(1):20386.
[44] Ansari S, et al. Eur Phys J Spec Top 2021;230(16):3273–80.
[45] Watts DJ. Amer J Soc 1999;105(2):493–527.
[46] Newman MEJ. J Stat Phys 2000;101:819–41.
[47] Newman MEJ. SIAM Rev 2003;45(2):167–256.
[48] Block P, et al. Nat Hum Behav 2020;4(6):588–96.
[49] Thurner S, Klimek P, Hanel R. Proc Natl Acad Sci 2020;117(37):22684–9.
[50] Bjørnstad ON. Epidemics: models and data using R. Springer Nature; 2022.
[51] Delamater PL, et al. Emerg Infect Dis 2019;25(1):1.
[52] Mugnaine M, et al. Chaos Solitons Fractals 2022;155:111784.
[53] Moore C, Newman MEJ. Phys Rev E 2000;61(5):5678.
[54] Kuperman M, Abramson G. Phys Rev Lett 2001;86(13):2909.
[55] Zanette DH, Kuperman M. Physica A 2002;309(3–4):445–52.
[56] Verdasca J, et al. J Theoret Biol 2005;233(4):553–61.
[57] Gama MMTd, Nunes A. Eur Phys J B 2006;50:205–8.
[58] Han XP. Phys Lett A 2007;365(1–2):1–5.
[59] Li X, Wang X. Internat J Systems Sci 2007;38(5):401–11.
[60] Shanker O, Hogg T. Modern Phys Lett B 2009;23(10):1249–62.
[61] Xu Z, Sui DZ. Geogr Anal 2009;41(3):263–82.
[62] Vieira IT, Senna Vd, Pereira HBdB. Pesqui Oper 2011;17.
[63] Liu M, et al. PLoS One 2015;10(3):9.
[64] Zhan XX, et al. Appl Math Comput 2018;332:437–48.
[65] Milgram S. Psychol Today 1967;2(1):60–7.
[66] Watts DJ, Strogatz SH. Nature 1998;393(6684):440–2.
[67] Watts DJ. Small worlds: the dynamics of networks between order and randomness. Princeton University Press; 2004.
[68] Hindmarch AC. IMACS Trans Sci Comput 1983;1:55–64.